DM-COM: Combining Device-to-Device and MU-MIMO Communications for Cellular Networks

Pedram Kheirkhah Sangdeh, Hossein Pirayesh, Qiben Yan, and Huacheng Zeng

***Abstract*—In cellular networks, multi-user MIMO (MU-MIMO) is a key technology and has already been deployed in many real systems. Recently, device-to-device (D2D) communication has emerged as another promising technology as it offers several advantages, such as traffic offloading, low-latency transmissions, and enhanced spectral efficiency. Although there are many results of these two technologies, most of them are limited to their respective domains and there is a lack of practical design to combine both technologies for cellular networks. In this paper, we present DM-COM, a practical scheme for enabling the coexistence of D2D and MU-MIMO subsystems in cellular networks. The enabler of DM-COM is a new approach for managing the mutual interference between the two subsystems, which does not require channel state information and is therefore amenable to practical implementation. We have built a prototype of DM-COM on a wireless testbed and evaluated its performance in a real-world wireless environment. Our experimental results show that, using DM-COM in a small cellular network, D2D users achieve 1.9 bit/s/Hz spectral efficiency, while MU-MIMO users have less than 8% throughput degradation compared to the case without D2D users.**

***Index Terms*—Device-to-Device communications, multi-user MIMO, cellular networks, 5G NR, Internet of things.**

I. Introduction

Cellular networks are key components of the telecommunications infrastructure in our society. Their role of providing ubiquitous wireless Internet services becomes increasingly important with the proliferation of Internet-based applications such as smart cities, the Internet of things (IoT), and autonomous driving. To increase the network capacity, provide massive connectivity, and meet the growing demands for wireless services, many advanced wireless technologies have been proposed for next-generation cellular networks. Multi-user multiple-input multiple-output (MU-MIMO), which allows a multi-antenna base station (BS) to simultaneously serve multiple user equipment (UEs) on the same spectrum band, is one of the pivotal technologies for cellular networks [1]. As its benefits are well recognized, MU-MIMO has already been deployed in real cellular networks to harness its throughput gain in the presence of antenna configuration asymmetricity.

Device-to-device (D2D) communication is another promising technology for cellular networks [2]. Its basic idea is to allow direct communication between two proximity-based mobile users without traversing the BS or core network. As mobile users in today's cellular networks require high data rate services (e.g., video sharing, online gaming, proximity-aware networking) in which they could potentially be in a short range for direct communication, D2D communication can greatly increase the spectral efficiency of the network. Moreover, the advantages of D2D communication go beyond spectral efficiency. Saving the airtime at the core network, D2D communication offers more airtime to the BS that can be leveraged to serve a massive number of low-rate devices such as IoT sensors. It also can potentially reduce packet transmission delay, enhance user fairness, offload traffic for BSs, and alleviate congestion for core networks, especially in networks congested by IoT devices [3].

Although there are many results of MU-MIMO and D2D communications [4]–[28], most of them are limited to their respective domains and there is a lack of practical design to harvest the benefits of both technologies in cellular networks. Such a stagnation underscores the critical need for bridging this gap. The main challenge in such a joint design is the interference management between MU-MIMO devices (BS and UEs) and D2D devices. As existing MU-MIMO schemes are vulnerable to interference (e.g., pilot contamination), the performance of MU-MIMO communication will be dramatically degraded by interference from active D2D devices if interference is not properly handled. At the same time, interference from MU-MIMO devices will also disrupt the D2D communications. Therefore, the coexistence of D2D and MU-MIMO communications necessitates a systematic scheme to tame the mutual interference between the two subsystems.

In this paper, we present DM-COM, a practical scheme for enabling the coexistence of D2D and MU-MIMO communications for cellular networks. We consider a single cell that comprises a BS, a set of cellular UEs (C-UEs), and a pair of D2D UEs (D-UEs) on each physical resource block (PRB). The BS is equipped with several antennas; the C-UEs are equipped with one antenna; and the D-UEs are equipped with one or multiple antennas. MU-MIMO is used for communication between the BS and set of C-UEs. D2D technology is used for communication between the pair of D-UEs. We assume that MU-MIMO communication follows the principles of 5G new radio (NR) standard (e.g., waveform and frame structure). We also assume that D-UEs know the network protocol and transmission pattern used by MU-MIMO as such information will be broadcast by BS over control channel. We further assume that the D2D applications are sensitive to communication latency (e.g., virtual reality, online gaming, and health monitoring) and thus require low-delay bidirectional transmissions. In such a network, our objective is to enable the concurrent spectrum utilization of MU-MIMO

The authors are with the Department of Computer Science and Engineering, Michigan State University, East Lansing, MI 48824 (e-mail:hzeng@msu.edu).
This work was supported in part by the NSF grants CNS-2100112, CNS-2113618, CNS-1950171, and CNS-1949753.

and D2D communications.

Toward this objective, we employ a blend of two interference management techniques: interference cancellation and beamforming, which are used in the following way. In the uplink MU-MIMO, the BS receives both desired signals from C-UEs and interfering signals from D-UEs. To decode its desired signals, the BS leverages the spatial degrees of freedom (DoF) provided by its multiple antennas and constructs a decoding matrix to cancel interference and equalize the channel distortion. In the downlink MU-MIMO, the BS constructs a beamforming (precoding) matrix to send its intended signals to C-UEs while pre-canceling interference for the receiving D-UEs. The C-UEs do not participate in the interference management and, instead, they rely on other devices to handle their interference. A similar approach is adopted to manage interference in the D2D subsystem.

While the idea of our interference management scheme is clear, many technical issues remain challenging. For uplink MU-MIMO transmission, how can the BS decode the signals from C-UEs in the presence of interference from D-UEs? For downlink MU-MIMO transmission, how can the BS perform beamforming in the downlink so it can mute its interference for the D-UEs? For these two questions, one possible solution is to design a dedicated channel acquisition protocol for the BS to obtain channel state information (CSI) for signal detection and beamforming. However, such a solution not only entails a large airtime overhead but also complicates the system operation. In light of this, we propose a new MU-MIMO scheme that is resilient to interference from/to D-UEs. The key idea of our new scheme is that, instead of relying on CSI for signal detection and beamforming, we blindly use the received signals to extract spatial information required to train decoding and beamforming matrices. Surprisingly, such a scheme leads to a very good performance for signal detection in the face of interference, provided that the BS has sufficient antennas.

For the D2D communication, we apply the same approach to managing interference. Specifically, for a transmitting D-UE, it leverages the overheard interference from C-UEs to construct the precoding matrix for beamforming. For a receiving D-UE, it leverages the reference signals to construct the decoding matrix for signal detection in the presence of interference. By doing so, the D-UEs do not require CSI for signal detection and beamforming. Therefore, the need for notorious channel feedback is eliminated.

Based on the above interference management scheme, we have developed DM-COM to enable the coexistence of D2D and MU-MIMO communications in cellular networks. In a nutshell, DM-COM advances the state-of-the-art in the following aspects:

- At the cellular BS, we have designed an interference management technique that cancels interference from/to D2D users at uplink/downlink. This scheme does not need CSI nor synchronization with D2D users.
- At the D2D users, we have designed an interference management technique that cancels interference from/to cellular nodes. This scheme does not need CSI nor synchronization with cellular subsystem.
- We have proposed DM-COM, a holistic scheme to enable coexistence of D2D and MU-MIMO technologies without adversely affecting each other.
- We have built a prototype of DM-COM on a wireless testbed consisting of USRP N210 devices and shown DM-COM's efficacy in handling cross-subsystem interference in real-world wireless environment.

We have evaluated the performance of DM-COM in a picocell network where a four-antenna BS serves two single-antenna C-UEs in accordance with 5G NR standard. In the network, there coexists a pair of D-UEs for direct communication. One D-UE has one antenna and the other has three antennas. Our experimental results show that DM-COM reaches 1.9 bit/s/Hz spectral efficiency for D2D users. This is achieved at the cost of 8.0% throughput degradation for MU-MIMO users (compared to the case without D2D users). Moreover, compared to the conventional case where all the users (C-UEs and D-UEs) are served by the BS, DM-COM improves the average network throughput from 21.9 Mbps to 35.1 Mbps in 5 MHz bandwidth, i.e., 60.3% throughput gain for DM-COM is observed. Our experimental results show that DM-COM successfully re-uses the spectrum that is pre-occupied by C-UEs. DM-COM maintains the performance of incumbent C-UEs and increases the overall network throughput through establishing D2D communications.

II. Related Work

We briefly review D2D and MU-MIMO solutions in cellular networks.

D2D: To accommodate ever-increasing users in cellular networks and enhance the spectrum re-utilization, D2D users are allowed to communicate directly without involvement of the BS. Despite its potential benefits, a D2D sub-system needs to control co-channel interference, manage resources for competing users, and mitigate security threats [3]. In order for accomplishing these tasks, the enablers of D2D communications are beamforming [4]–[6], spectral resource management [7]–[10], power control [7], [11]–[16], and mode selection [17]–[19]. The existing research efforts follow different objectives, such as achievable data rate maximization [7], [15]–[18], fairness [13], interference minimization [14], energy efficiency [4], [9]–[12], and security of D2D systems [20]–[22]. From another perspective, most of existing works consider spectrum re-utilization in either uplink (see, e.g., [13]–[15]) or downlink (see, e.g., [4]–[6]) of cellular networks, but not both.

Moreover, most of the existing works require perfect global channel knowledge as well as network-wide synchronization. In contrast, DM-COM enables spectrum re-utilization in both uplink and downlink. It does not require channel feedback between the network devices, nor network-wide fine-grained synchronization.

MU-MIMO: MU-MIMO has widely been employed in current wireless systems. The main components of MU-MIMO are beamforming in the downlink and multi-user detection in the uplink. Most of beamforming methods are reliant on perfect CSI [23]–[25]. In the uplink, blind beamforming

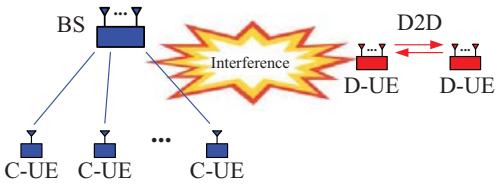

Fig. 1: Coexisting MU-MIMO and D2D communications over one PRB in a cellular network.

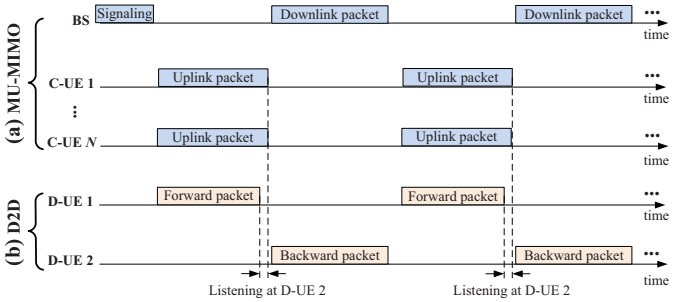

Fig. 2: The proposed network protocol for coexisting MU-MIMO and D2D communications.

methods offer a solution to this challenge, but suffer from high computational complexity and long processing delays since they need to solve a complex optimization problem [26]–[28] or follow sophisticated procedures to learn spatial information [29]–[31]. In the downlink, existing signal detection methods consider benign environments where the network nodes are perfectly synchronized [32]–[35]. DM-COM differs from existing methods as it eliminates the need for channel feedback and network-wide synchronization in both downlink and uplink.

III. Problem Description

Network Setting: We consider a cellular network as shown in Figure 1. It comprises a BS, a set of C-UEs, and a pair of D-UEs on one PRB. The BS has multiple antennas, and each C-UE has a single antenna.[1] Let M_{bs} denote the number of the BS's antennas. Let N denote the number of C-UEs. To fully utilize the BS's antennas and maximize the spectral efficiency, MU-MIMO is used for the communication between the BS and N C-UEs. The BS coordinates uplink and downlink transmissions with time division multiple access (TDMA) to serve cellular users. Within the cellular network, there coexists a pair of D-UEs intending to conduct bi-directional communication over a PRB without traversing the BS. Without any loss of generality, in the remainder of this paper, we focus on one pair of D-UEs over a PRB. All the arguments hold for multiple pairs of D-UEs, each of which exclusively works over one or multiple PRBs. In the D2D pair under consideration, the two D-UEs may have different numbers of antennas. Let M_{d1} and M_{d2} denote the number of D-UE 1's and D-UE 2's antennas, respectively. Without loss of generality, we also assume that the number of D-UE 1's antennas is less than or equal to the number of D-UE 2's antennas, i.e., $M_{\text{d1}} \leq M_{\text{d2}}$. For such a network, we have the following assumptions and justifications:

- We assume that the user selection for MU-MIMO and D2D has taken place. User selection is not within the scope of this work. In real networks, there may exist multiple pairs of D-UEs. In that case, different pairs of D-UEs can be assigned to different PRBs based on some criteria. So, focusing on one pair is sufficient to study the coexistence problem which is indeed the main objective of this paper.
- We assume that the BS has more antennas than C-UEs, i.e., $M_{\text{bs}} > N$. This assumption can be fulfilled through user selection algorithms. Under this assumption, in addition to decoding the N desired data streams from C-UEs, the BS has remaining spatial DoF provided by its antennas to cancel interference from/to D-UEs.
- We assume that the D-UEs know the data flow pattern of MU-MIMO communication indicated by slot format in NR. We also assume that C-UEs are oblivious to D-UEs. C-UEs will not contribute to the interference management.
- We assume that the channel coherence time is sufficient (e.g., 1 ms). The same assumption has been made by other beamforming-based MIMO systems [23]–[25].

Our Objective: We aim to develop DM-COM, a practical scheme to enable the coexistence (concurrent spectrum utilization) of D2D and MU-MIMO communications by taming their mutual interference. More specifically, we aim to maximize the throughput of the D2D communication while maintaining the performance of MU-MIMO subsystem.

IV. DM-COM: An Overview

In this section, we first present a network protocol for the concurrent spectrum utilization of coexisting MU-MIMO and D2D subsystems, and then analyze the achievable data streams on the D2D link. Finally, we point out the underlying challenges in interference management at the physical layer and outline our solutions.

A. Network Protocols

MU-MIMO Communication: In the context of cellular networks, Figure 2(a) presents our protocol for uplink and downlink MU-MIMO transmissions. The protocol works as follows. The BS first broadcasts an announcement about MU-MIMO transmission to the selected C-UEs. Then, the selected C-UEs send their packets to the BS in the uplink, which is followed by spatial multiplexing in downlink transmissions. The uplink and downlink transmissions repeat until the session of MU-MIMO communication terminates.

To support MU-MIMO communication, we consider NR-like frame format. Figure 3 depicts the frame structure in one PRB within a frame. To be specific, this frame structure is adopted based on N38 frequency band and slot format 45 setting over 5 MHz [36]. As shown in the figure, the frame is composed of 10 subframes, each of which comprises 14

[1]DM-COM can support the case where C-UE has multiple antennas by simply treating a multi-antenna C-UE as multiple single-antenna C-UEs.

OFDM symbols according to numerology $\mu = 0$ in NR. Based on the bandwidth configuration, an OFDM symbol has 300 occupied subcarriers grouped into 25 PRBs.

Reference signals are embedded into frames for synchronization, signal demodulation, phase tracking, etc. Among the reference signals shown in Fig. 3, We will leverage PDSCH DM-RS of downlink packets and PUSCH DM-RS of uplink packets in our design. As shown in the figure, not every subcarrier has these reference signals. This is because, the subcarrier spacing is small (15 kHz), and the channels of adjacent subcarriers are highly correlated. Therefore, if a subcarrier does not have reference signal, the reference signals on its adjacent subcarriers can be used for signal demodulation (detection). This feature will also be leveraged in the design of our signal detection method. Time division duplex (TDD) is considered for MU-MIMO to support its uplink and downlink transmissions. The ratio of uplink and downlink duration can be configured as desired based on the slot format. For ease of demonstration, we have considered slot format 45 with equal downlink/uplink duration, and we equally assigned flexible OFDM symbols to uplink and downlink transmissions.

D2D Communication: Figure 2(b) shows the proposed transmission protocol for the D2D communication, with respect to the timeline of uplink/downlink transmission in MU-MIMO subsystem. In uplink MU-MIMO, D2D conducts forward transmissions (from D-UE 1 to D-UE 2). In downlink MU-MIMO, D2D conducts backward transmissions (from D-UE 2 to D-UE 1). To establish such a timing alignment, D2D subsystem needs neither fine-grained synchronization with MU-MIMO subsystem nor coordination from the cellular BS. The D2D subsystem can learn cellular traffic pattern by either listening the information over the control channel or tracking the spatial signatures of signals on multiple antennas on D-UEs. It then adjusts its transmission activities based on learned pattern. As illustrated in the figure, the time duration of D2D forward transmissions is slightly shorter than that of uplink MU-MIMO. In this time period, D-UE 2 overhears the interfering signals from C-UEs, which will be used for the calculation of its beamforming matrix.

For the D2D communication, two remarks are in order. First, mutual interference between D2D and MU-MIMO communications will be properly handled at the physical layer. Therefore, the D2D and MU-MIMO subsystems remain oblivious to each other from the viewpoint of MAC or upper layers. Second, as we shall see later, the interference management at the physical layer does not require PHY-layer cooperation between the D2D and MU-MIMO subsystems. Hence, the D2D and MU-MIMO subsystems do not need to use the same frame structure and modulation. As we will show via experiments, D2D can employ IEEE 802.11 PHY for its transmissions.

B. Achievable Data Streams (DoF) on the D2D Link

For the protocol in Figure 2, a natural question to ask is how many data streams can be transported on the D2D link. Apparently, it depends on the number of D-UE 2's antennas. If D-UE 2 has a large number of antennas, then many data

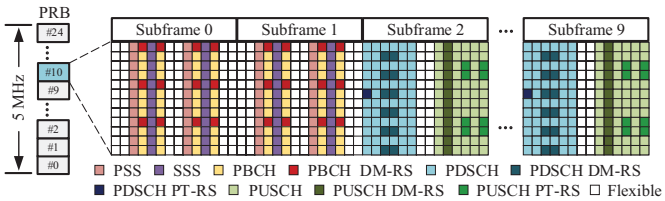

Fig. 3: Frame structure for MU-MIMO communication.

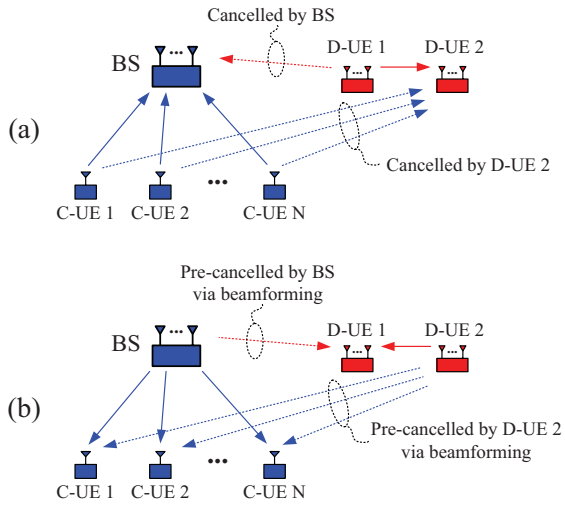

Fig. 4: Illustrating the mutual interference between MU-MIMO and D2D subsystems: (a) uplink; (b) downlink.

streams can be transported on the D2D link, provided that D-UE 1 has enough DoF to support all incoming streams from D-UE 2. If D-UE 2 does not have sufficient antennas, then no data stream can be transported on the D2D link. We note that the number of data streams on an MIMO link, which is also known as DoF, is the first-order approximation of its Shannon capacity with respect to SNR. It also represents the multiplexing gain of the MIMO link in high-SNR regime. Therefore, studying the number of data streams is of great theoretical importance to analyze the achievable data rate of the D2D link (given that analyzing its Shannon capacity is out of our capability). In what follows, we derive the achievable data streams on the D2D link by analyzing the spatial DoF consumption in the uplink and downlink MU-MIMO using an existing DoF model [37].

Assume that the bi-directional transmissions on the D2D link are symmetric, i.e., the number of data streams from D-UE 1 to D-UE 2 is the same as that from D-UE 2 to D-UE 1. We let $d \in \mathbb{N}_0$ denote the number of data streams on the D2D link. To determine the maximum value of d, we first consider the uplink MU-MIMO as shown in Figure 4(a). At the BS, it needs to decode N data streams from C-UEs and cancel d interfering streams from D-UE 1. Based on the DoF model in [37], we have $N + d \leq M_{\text{bs}}$. At D-UE 1, it needs to transmit d data streams. We therefore have $d \leq M_{\text{d1}}$. At D-UE 2, it needs to decode d data streams and cancel N data streams from C-UEs. We have $N + d \leq M_{\text{d2}}$. Based on the above three constraints, the maximum number of achievable

data streams on the D2D link can be expressed by

$$d = \min(M_{d1}, M_{d2} - N, M_{\rm bs} - N)_+, \quad (1)$$

where $(\cdot)_+$ returns a nonnegative number, i.e., $\max(\cdot, 0)$. By the same token, it is easy to verify that d in (1) is also the maximum number of achievable data streams on the D2D link in downlink MU-MIMO (see Figure 4(b)).

C. Interference Management and Its Challenges

Now, the question is how to handle interference at the physical layer so that the D2D link can achieve d data streams while the MU-MIMO subsystem can maintain its N data streams between the BS and the N C-UEs. To answer this question, we consider uplink and downlink MU-MIMO separately. For the uplink as shown in Figure 4(a), we need to design a signal detection method for both D-UE 2 and the BS so that they can decode their respective signals in the presence of interference from unintended transmitters. For the downlink as shown in Figure 4(b), we need to design a beamforming method for both D-UE 2 and the BS so that they can pre-cancel their generated interference for their unintended receivers.

While there are many results of signal detection and beamforming in the context of MIMO, most of them require global CSI and perfect synchronization. Such requirements entail a large amount of airtime overhead, thereby degrading the spectral efficiency and complicating system operation. In light of this challenge, we propose a new signal detection method and show its resilience to interference. In contrast to existing detection methods (e.g., zero-forcing and minimum mean square (MMSE) detectors), our signal detection method does not require CSI but is capable of decoding signals in the face of interference. In the downlink, we propose two new beamforming methods for BS and D-UE 2, respectively. Again, the proposed beamforming methods do not require CSI for the design of precoding matrix, differentiating themselves from existing beamforming methods.

V. MU-MIMO Communication

In this section, we present new signal detection and beamforming methods for MU-MIMO to handle interference between the BS and D-UE 1 (see Figure 4). Interference between C-UEs and D-UE 2 will be handled by the D2D communication method presented in the next section.

A. Basic Idea

In the MU-MIMO subsystem, the BS handles its interference in both uplink and downlink transmissions by leveraging its spatial DoF offered by multiple antennas. Specifically, in the uplink MU-MIMO as shown in Figure 4(a), the BS performs interference cancellation and signal detection to recover its desired signals from the N C-UEs in the presence of interference from D-UE 1. At the BS, interference cancellation and signal detection will be done using spatial matrices to combine the received signals from its multiple antennas. In the downlink MU-MIMO as shown in Figure 4(b), the BS applies beamforming to pre-cancel its generated interference at D-UE 1. Recall that we assume the BS has more antennas than C-UEs ($M_{\rm bs} > N$). This assumption ensures that the BS has sufficient spatial DoF to send N data streams toward the N C-UEs and, at the same time, it is able to nullify its generated interference at D-UE 1.

In contrast to the BS, the C-UEs do not participate in the interference management since they have a single antenna. They will rely on D-UE 2 to handle interference in both uplink and downlink. As such, DM-COM preserves the backward compatibility with incumbent C-UEs. In what follows, we focus on the baseband signal processing at the BS. We first present the signal detection method for the uplink and then present the beamforming method for the downlink.

B. Uplink Signal Detection at the BS

Mathematical Formulation: We consider the uplink MU-MIMO transmissions in the presence of interference from D-UE 1 as shown in Figure 4. Let $\mathbf{s}_{\rm c} \in \mathbb{C}^{N\times 1}$ denote the vector of signals that are transmitted by the N C-UEs. Let $\mathbf{s}_{\rm d} \in \mathbb{C}^{d\times 1}$ denote the vector of signals that are transmitted by D-UE 1. Let $\mathbf{P}_{\rm d} \in \mathbb{C}^{M_{\rm d1}\times d}$ denote its precoding vector. Also, $\mathbf{H}_{\rm c} \in \mathbb{C}^{M_{\rm bs}\times N}$ denotes the compound channel between the BS and the N C-UEs, and $\mathbf{H}_{\rm d} \in \mathbb{C}^{M_{\rm bs}\times M_{\rm d1}}$ stands for the MIMO channel between the BS and D-UE 1. We further let $\mathbf{w} \in \mathbb{C}^{M_{\rm bs}\times 1}$ denote noise at the receiving BS. Then, the vector of received signals at the BS, which we denote as $\mathbf{y} \in \mathbb{C}^{M_{\rm bs}\times 1}$, can be written as:

$$\mathbf{y} = \mathbf{H}_{\rm c}\mathbf{s}_{\rm c} + \mathbf{H}_{\rm d}\mathbf{P}_{\rm d}\mathbf{s}_{\rm d} + \mathbf{w}. \quad (2)$$

At the BS, to recover its desired signal $\mathbf{s}_{\rm c}$ in the presence of interfering signal $\mathbf{s}_{\rm d}$ and noise $\mathbf{w}$, one approach is using conventional MIMO detectors, such as zero-forcing and MMSE detectors. These approaches, however, require channel knowledge about $\mathbf{H}_{\rm c}$ and $\mathbf{H}_{\rm d}$. While $\mathbf{H}_{\rm c}$ is easy to obtain, $\mathbf{H}_{\rm d}$ is not. If the BS intends to obtain $\mathbf{H}_{\rm d}$, it requires to cooperatively work with D-UE 1, and a dedicated protocol is needed for channel sounding as well. This increases the airtime overhead and complicates network operation remarkably. In light of this challenge, we propose an approximate-MMSE MIMO detector for the BS, which does not require channel knowledge about $\mathbf{H}_{\rm c}$ and $\mathbf{H}_{\rm d}$ for signal detection.

Detection Matrix Design: We consider linear detection at the BS. By letting $\mathbf{G} \in \mathbb{C}^{N\times M_{\rm bs}}$ denote the detection matrix, the estimated signal at the BS can be written as $\hat{\mathbf{s}}_{\rm c} = \mathbf{G}\mathbf{y}$, where $\hat{\mathbf{s}}_{\rm c}$ is the estimated version of signal $\mathbf{s}_{\rm c}$. Then, the mean square error (MSE) between the original signal $\mathbf{s}_{\rm c}$ and estimated signal $\hat{\mathbf{s}}_{\rm c}$ can be written as: $\mathrm{MSE} = \mathbb{E}\big[|\mathbf{G}\mathbf{y} - \mathbf{s}_{\rm c}|^2\big]$, where $|\cdot|^2$ is ℓ^2-norm of a complex vector. By letting $\frac{\partial \mathrm{MSE}}{\partial \mathbf{G}} = \mathbf{0}$, we can obtain $\mathbf{G} = \mathbb{E}[\mathbf{s}_{\rm c}\mathbf{y}^{\sf H}]\mathbb{E}[\mathbf{y}\mathbf{y}^{\sf H}]^+$, where $[\cdot]^+$ is Moore-Penrose inverse. This is actually another form of MMSE MIMO detector.[2]

To calculate $\mathbf{G}$ in real systems, we need to compute $\mathbb{E}[\mathbf{s}_{\rm c}\mathbf{y}^{\sf H}]$ and $\mathbb{E}[\mathbf{y}\mathbf{y}^{\sf H}]$. To do so, we take advantage of the demodulation

[2]By letting $\mathbf{H}$ denote the compound channel and assuming that the distribution of transmit signal is i.i.d., $\mathbf{G}$ can be transformed to its classical form: $\mathbf{G} = \mathbb{E}[\mathbf{s}_{\rm c}\mathbf{y}^{\sf H}]\mathbb{E}[\mathbf{y}\mathbf{y}^{\sf H}]^+ = \mathbf{H}^{\sf H}(\mathbf{H}\mathbf{H}^{\sf H} + \sigma^2\mathbf{I})^{-1}$, where σ^2 is the normalized noise power.

reference signals for uplink (PUSCH DM-RS) in the frame structure, as shown in Figure 3. In the uplink frame, one OFDM symbol is used for PUSCH DM-RS within a PRB. We can use these reference signals to estimate $\mathbb{E}[\mathbf{y}\mathbf{y}^{\mathsf{H}}]$ and $\mathbb{E}[\mathbf{y}\mathbf{s}_{\mathrm{c}}^{\mathsf{H}}]$. Let us define that a PRB has 12 subcarriers and 14 OFDM symbols. Let $\mathcal{R}$ denote the set of PUSCH DM-RS elements in an uplink PRB as shown in Figure 3. Let k and l denote the index of subcarriers and OFDM symbols, respectively. Then, we have $\mathbb{E}[\mathbf{y}\mathbf{y}^{\mathsf{H}}] \approx \frac{1}{|\mathcal{R}|}\sum_{(l,k)\in\mathcal{R}} \mathbf{y}(l,k)\mathbf{y}(l,k)^{\mathsf{H}}$ and $\mathbb{E}[\mathbf{s}_{\mathrm{c}}\mathbf{y}^{\mathsf{H}}] \approx \frac{1}{|\mathcal{R}|}\sum_{(l,k)\in\mathcal{R}} \mathbf{s}_{\mathrm{c}}(l,k)\mathbf{y}(l,k)^{\mathsf{H}}$. Consequently, $\mathbf{G}$ can be approximately expressed as:

$$\mathbf{G} = \Big[\sum_{(l,k)\in\mathcal{R}} \mathbf{s}_{\mathrm{c}}(l,k)\mathbf{y}(l,k)^{\mathsf{H}}\Big]\Big[\sum_{(l,k)\in\mathcal{R}} \mathbf{y}(l,k)\mathbf{y}(l,k)^{\mathsf{H}}\Big]^{+}, \quad (3)$$

where $\mathbf{s}_{\mathrm{c}}(l,k)$, $(l,k)\in\mathcal{R}$, is a PUSCH DM-RS element at the N C-UEs; and $\mathbf{y}(l,k)$, $(l,k)\in\mathcal{R}$, is the corresponding received signal at the BS, which includes both PUSCH DM-RS element from the C-UEs and interfering signals from D-UE 1. We note that in (3), we replace the approximation sign ($\approx$) with equation sign ($=$) for simplicity. We also note that, since $\mathbf{G}$ in (3) is an approximation of MMSE MIMO detector, we therefore term it approximate-MMSE MIMO detector.

Performance Analysis: The approximate-MMSE MIMO detector does not require CSI for the signal detection. Instead, it uses the transmitted and received reference signals to compute the detection matrix. For this reason, the approximate-MMSE MIMO detector can decode desired signals in the presence of unknown interference.

It is interesting to explore the performance of this approximate-MMSE MIMO detector in the cellular network. Let us assume that the signals in a PRB experience the same channel, i.e., channel coherence frequency is greater than 12 subcarriers (180 kHz) and channel coherence time is greater than 14 OFDM symbols (1 ms). Let us further assume that noise is negligible (i.e., zero-noise regime). We have the following lemma:

Lemma 1: If th BS is equipped with sufficient number of antennas then the approximate-MMSE MIMO detector at BS can perfectly decode the signals from the N C-UEs, i.e., $\hat{\mathbf{s}}_{\mathrm{c}}(l,k) = \mathbf{s}_{\mathrm{c}}(l,k)$, $\forall l,k$.

The proof of this lemma is provided at Appendix A. This lemma shows the superior performance of approximate-MMSE MIMO detector in ideal scenarios (frequency-flat channel, sufficiently large channel coherence time, and zero-noise regime). For its performance in non-ideal scenarios, we resort to experimentation. Our experimental results in Section VII will show that the approximate-MMSE MIMO detector yields a good performance in real network scenarios.

C. Downlink Beamforming at BS

Beamforming Matrix Design: We now consider the beamforming for downlink MU-MIMO as shown in Figure 4(b). Based on the network information theory, if a network can send N data streams in the uplink, it can also send N data streams in the downlink. This principle inspires us in the design of beamforming matrix. Our beamforming method is simple – we use the detection matrix derived in the uplink as the beamforming matrix in the downlink. Let $\mathbf{z}(l,k) \in \mathbb{C}^{N\times 1}$ denote the vector of signals in OFDM symbol l on subcarrier k that the BS wants to send toward N C-UEs. Let $\mathbf{x}(l,k) \in \mathbb{C}^{M_{\mathrm{bs}}\times 1}$ denote the vector of precoded signals in OFDM symbol l on subcarrier k that the BS sends to its M_{bs} antenna ports. Then, the beamforming operation can be expressed as: $\mathbf{x}(l,k) = \alpha\mathbf{G}^{\mathsf{T}}\mathbf{z}(l,k)$, $\forall l,k$, where $\mathbf{G}$ is obtained in the uplink and $\alpha\in\mathbb{R}$ is a scaling factor to meet the requirement of the BS's transmit power.

In Lemma 1, we showed that the $\mathbf{G}$ matrix can perfectly recover the desired signals at the BS in the uplink. If the uplink and downlink channels reciprocity is maintained, it is evident that the C-UEs can also perfectly recover their respective signals in the downlink. Moreover, the BS can perfectly pre-cancel interference for D-UE 1, which is a receiver in this time period (see Figure 4(b)). For the beamforming method in non-ideal scenarios, we leave its performance evaluation to our experimental results in Section VII.

Channel Calibration: The proposed beamforming method relies on the channel reciprocity. For its deployment in real systems, relative channel calibration at the BS can be implemented to maintain the channel reciprocity. In our experiments, the relative calibration method in [38] is implemented at the BS as a part of beamforming implementation.

D. Discussions on Its Limitations

Two remarks on this MU-MIMO method are in order.

First, channel coherence time plays a critical role in the proposed MU-MIMO method. Suppose that both uplink and downlink occupy one subframe (1 ms). Then, the required channel coherence time should be longer than 1 ms. This is a mild requirement in real wireless environments.

Second, the performance of the proposed MU-MIMO method is dependent on the number of reference signals in an uplink PRB. Per our experiments, when a device has N_{ant} antennas, $\mathcal{R}$ needs to be selected such that $|\mathcal{R}| \geq 2N_{\mathrm{ant}}$. In this case, the average EVM gap between approximate-MMSE and ideal MMSE detectors is less than 3 dB. As such, D2D and MU-MIMO subsystems individually set an appropriate $\mathcal{R}$ and PUSCH DM-RS pattern to meet their own needs. For instance, $\mathcal{R}$ may embrace more than one PRB or PUSCH DM-RS pattern may entail dense distribution of reference signals to meet the requirements of D-UEs and the BS.

VI. D2D Communication

In this section, we focus on the D2D communication. As interference related to D-UE 1 has been tamed by the BS, we now focus on interference related to D-UE 2. Specifically, we design a D2D communication scheme such that D-UE 2 can properly handle its related interference in both uplink and downlink. A proper D2D scheme has to address the following two questions: For the uplink shown in Figure 4(a), how can D-UE 2 decode its intended signals in the presence of interference from C-UEs? For the downlink in Figure 4(b), how can D-UE 2 send its signal to D-UE 1 while pre-canceling its generated interference for C-UEs? In what follows, we present our solutions to these questions.

A. Signal Detection at D-UE 2

Referring to D2D forward transmissions in Figure 4(a), we follow the same approach presented in Section V-B for D-UE 2 to decode its signals in the presence of interference from C-UEs. Specifically, D-UE 2 first calculates a detection matrix using (3) and then uses the calculated detection matrix to filter out interference from C-UEs and equalize the channel distortion for signal recovery. The remaining question is what frame structure should be used for the D2D transmission. Actually, the frame structure for D2D transmission is flexible. As we will show in our experiments, the frame structure of D2D communication can be the same as the MU-MIMO frame structure as shown in Figure 3; it also can be IEEE 802.11 frame structure (consisting of preamble and data parts [39]).

B. Beamforming at D-UE 2

We now consider the D2D backward transmissions in Figure 4(b). In this time period, D-UE 2 needs to perform beamforming to pre-cancel its interference for C-UEs. Our beamforming method takes advantage of the overheard interfering signals in the previous time period, as illustrated in Figure 2. By leveraging the overheard signals, D-UE 2 constructs a beamforming matrix for signal transmission. In what follows, we detail the construction of beamforming matrix at D-UE 2.

Beamforming Matrix Design: Referring to Figure 2, in a short time period at the end of uplink MU-MIMO, D-UE 1 does not transmit signal and thus D-UE 2 receives only interfering signals from C-UEs. Let $\mathbf{Y}_{\mathrm{d}} \in \mathbb{C}^{M_{\mathrm{d2}} \times 1}$ denote the received signals at D-UE 2 in this time period. Then, we have

$$\mathbf{y}_{\mathrm{d}} = \mathbf{H}_{\mathrm{dc}}\mathbf{s}_{\mathrm{c}} + \mathbf{W}_{\mathrm{d}}, \tag{4}$$

where $\mathbf{H}_{\mathrm{dc}} \in \mathbb{C}^{M_{\mathrm{d2}} \times N}$ is the channel between C-UEs and D-UE 2; $\mathbf{s}_{\mathrm{c}} \in \mathbb{C}^{N \times 1}$ is the vector of transmit signals at the N C-UEs; and $\mathbf{w}_{\mathrm{d}} \in \mathbb{C}^{M_{\mathrm{d2}} \times 1}$ is noise vector at D-UE 2.

Let $\mathbf{P}_{\mathrm{d}} \in \mathbb{C}^{M_{\mathrm{d2}} \times d}$ denote the precoding matrix at D-UE 2. Then, based on the received signal $\mathbf{Y}_{\mathrm{d}}$, we construct $\mathbf{P}_{\mathrm{d}}$ as:

$$\mathbf{P}_{\mathrm{d}} = \mathbf{U}(:, M_{\mathrm{d2}} - d + 1 : M_{\mathrm{d2}}), \tag{5}$$

where $\mathbf{U}(:, n : m)$ is a submatrix of $\mathbf{U}$, which is from $\mathbf{U}$'s nth column to mth column. $\mathbf{U}$ is computed by

$$[\mathbf{U}\ \mathbf{D}\ \mathbf{V}] = \mathrm{svd}(\mathbf{y}_{\mathrm{d}}\mathbf{y}_{\mathrm{d}}^{\mathsf{H}}), \tag{6}$$

where $\mathbf{D}$ and $\mathbf{V}$ are redundant outputs, and $\mathrm{svd}(\cdot)$ denotes singular value decomposition. Using (5) and (6), we compute a beamforming matrix $\mathbf{P}_{\mathrm{d}}$ for each subcarrier in the OFDM symbols. Then, $\mathbf{P}_{\mathrm{d}}$ is applied to the corresponding subcarrier for beamforming during D-UE 2's signal transmission. Since the matrix $\mathbf{P}_{\mathrm{d}}$ is computed using the uplink interfering signal, it necessitates channel reciprocity when using $\mathbf{P}_{\mathrm{d}}$ as the beamforming matrix in the downlink. Therefore, channel calibration has to been done at D-UE 2 in order to pre-cancel its interference for C-UEs. Again, RF calibration can be used at D-UE 2 in the baseband signal processing domain to preserve channel reciprocity.

Performance Analysis: We first study the performance of the proposed beamforming scheme in an ideal network scenario.

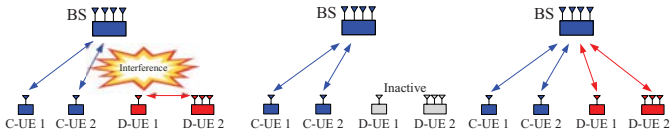

(a) DM-COM (b) Cellular-MU-MIMO (C) Full-MU-MIMO [t]

Fig. 5: Experimental setup and comparison baselines.

TABLE I: The parameters of experimental network.

	MU-MIMO subsystem	D2D subsystem 1	D2D subsystem 2
Standard	NR-like	NR-like	WiFi-like
Waveform	OFDM	OFDM	OFDM
FFT point	512	512	64
Valid subcarrier	300	300	52
Sample rate	5 Msps	5 Msps	5 Msps
Symbol duration	71.35 μs	71.35 μs	16 μs
Signal bandwidth	2.9 MHz	2.9 MHz	4 MHz
Carrier frequency	2.48 GHz	2.48 GHz	2.48 GHz
Transmit power	$\sim$ 18 dBm	$\sim$ 18 dBm	$\sim$ 18 dBm

Let us assume that all the MIMO channels have full rank. Let us assume that the channel coherence time is sufficiently large (larger than the time duration of downlink). Let us assume that the channel is perfectly calibrated at D-UE 2, i.e., the downlink and uplink channels are reciprocal. Let us further assume that noise is negligible, and D-UE 2 has sufficient number of antennas, i.e., $d + N \leq M_{\mathrm{d2}}$. Then, we have the following lemma:

Lemma 2: The constructed beamforming matrix $\mathbf{P}_{\mathrm{d}}$ can completely pre-cancel interference for the N C-UEs on every OFDM subcarrier.

The proof of Lemma 2 is provided in Appendix B. Lemma 2 shows the superior performance of the proposed beamforming method. It is worth noting that although the beamforming technique presented in Section V works for D-UE 2, we observed in experiments that the proposed SVD-based technique has superior performance in terms of interference leakage. In light ot this, the proposed technique is applied on D-UE 2 to preserve the performance of MU-MIMO subsystem.

VII. Experimental Evaluation

In this section, we build a prototype of DM-COM and evaluate its performance in a small network.

A. Implementation and Experimental Setup

Implementation: We have built a wireless network testbed that consists of a BS, two C-UEs, and two D-UEs as shown in Figure 5(a). The BS has four antennas. The C-UEs has one antenna. D-UE 1 has one antenna. D-UE 2 has three antennas. The BS, C-UEs, and D-UEs are built using USRP N210 devices as the radio transceivers and general-purpose computers as baseband signal processors.

We implement DM-COM on this testbed. The MU-MIMO subsystem is implemented using a custom-built 5G NR PHY, while the D2D subsystem is implemented using both NR-like and WiFi-like PHYs. The PHY parameters of DM-COM implementation are listed in Table I. Based on these PHYs,

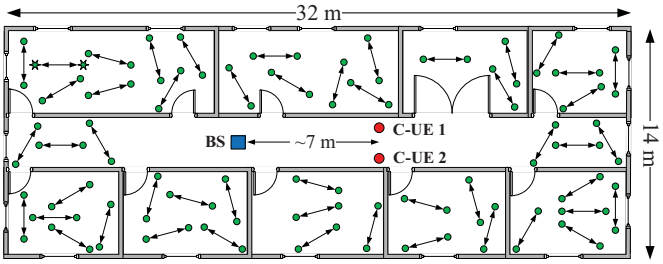

Fig. 6: The floor plan of our experiments.

TABLE II: EVM specification for NR-like PHY [40], [41].

EVM (dB)	$[-6.3, -9.1)$	$[-9.1, -11.8)$	$[-11.8, -14.2)$	$[-14.2, -16.8)$	$[-16.8, -19.1)$
CQI	6	7	8	9	10
Modulation	QPSK	16QAM	16QAM	16QAM	64QAM
Code rate $\times 1024$	602	378	490	616	466
γ(EVM)	1.1758	1.4766	1.9141	2.4063	2.7305
EVM (dB)	$[-19.1, -21.0)$	$[-21.0, -23.3)$	$[-23.3, -25.7)$	$[-25.7, -28.2)$	$[-28.2, -\infty)$
CQI	11	12	13	14	15
Modulation	64QAM	64QAM	64QAM	64QAM	64QAM
Code rate $\times 1024$	567	666	772	873	948
γ(EVM)	3.3223	3.9023	4.5234	5.1152	5.5547

we implement the MAC protocols for both MU-MIMO and D2D subsystems as shown in Figure 2. For the MU-MIMO protocol, both uplink and downlink transmissions have the same duration. For the D2D protocol, the time duration of "listening at D-UE 2" is about 71.35 µs.

Experimental Setup: Fig. 6 depicts the floor plan of our experiments. The BS and C-UEs are always placed on the spots marked by blue and red colors, respectively. The distance between BS and cellular users is about 7 m. D-UE 1 and D-UE 2 are deployed over 50 random locations in Figure 6. In each location, the distance between D-UEs is about 3 m. We use the indoor environments for ease of experimentation. Moreover, many small cells will be deployed in the buildings as mobile hotspots in the near future.

B. Performance Metrics and Comparison Baselines

Performance Metrics: We use two metrics to evaluate the performance of DM-COM. The first one is error Vector Magnitude (EVM), which is defined as follows: $\text{EVM} = 10\log_{10}(\frac{\mathbb{E}[|\hat{S}(l,k)-S(l,k)|^2]}{\mathbb{E}[|S(l,k)|^2]})$, where $\hat{S}(l,k)$ and $S(l,k)$ are the estimated and original signals, respectively. EVM is widely used in both IEEE 802.11 standards [39] and 3GPP standards [36] to measure quality of decoded signals, define modulation modulation and coding scheme (MCS), and estimate the achievable data rate as we see shortly.

The second metric is the achievable data rate. Based on the measured EVM, we extrapolate the achievable data rate using the MCS defined in the 3GPP standard and IEEE 802.11ac standard as follows: $r = \frac{1}{2}\cdot\frac{N_{\text{sc}}}{N_{\text{fft}}+N_{\text{cp}}}\cdot b\cdot\gamma\,(\text{EVM})$, where coefficient $1/2$ stems from halftime uplink and halftime downlink transmissions in MU-MIMO. N_{sc}, N_{fft}, and N_{cp} denote number of used subcarriers, FFT points, and the length of cyclic prefix, respectively. b is the sampling rate in Msps. $\gamma(\text{EVM})$ is the spectral efficiency of transmission based on MCS selection defined in standards. Table II and Table III present $\gamma\,(\text{EVM})$ for NR-like and WiFi-like PHYs, respectively.

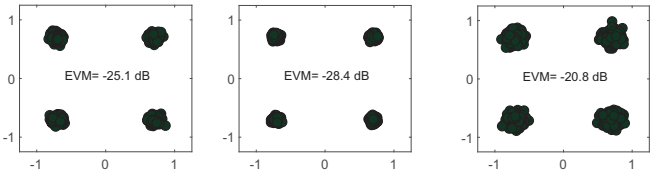

(a) Decoded signal from C-UE 1 at BS. (b) Decoded signal from C-UE 2 at BS. (c) Decoded signal from D-UE 1 at D-UE 2.

Fig. 7: Decoded (demodulated) signals in the MU-MIMO and D2D subsystems in the uplink/forward transmission.

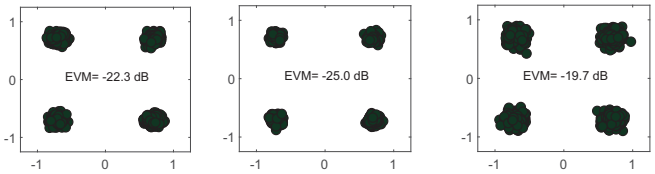

(a) Decoded signal from BS at C-UE 1. (b) Decoded signal from BS at C-UE 2. (c) Decoded signal from D-UE 2 at D-UE 1.

Fig. 8: Decoded (demodulated) signals in the MU-MIMO and D2D subsystems in the downlink/backward transmission.

Comparison Baselines: As shown in Figure 5, we compare DM-COM with two existing schemes: Cellular-MU-MIMO and Full-MU-MIMO. In the Cellular-MU-MIMO, the BS serves the two C-UEs only, and the two D-UEs are deactivated. In the Full-MU-MIMO, the BS serves the two C-UEs while the two D-UEs communicate with each other with the aid of BS. Technically, the BS simultaneously serves the four UEs in both uplink and downlink.

C. A Case Study of DM-COM

We first use a case study to scrutinize DM-COM and its interference cancellation capability. In this case study, we place the two D-UEs at two spots marked by stars in the upper-left room in Figure 6, and the D2D subsystem uses NR-like PHY for communications. Recall that DM-COM comprises two phases: uplink and downlink, as shown in Figure 4. In what follows, we first examine the decoded signals in the two phases and then study interference cancellation capability.

Constellation, EVM, and Data Rate: Referring to Figure 4(a), in the uplink, the BS demodulates the signals from the two C-UEs; at the same time, D-UE 2 demodulates the signal from D-UE 1. Figure 7 exhibits the constellation of the demodulated signals at the BS and D-UE 2, as well as their EVMs. Based on the measured EVM, the uplink data rates of C-UE 1 and C-UE 2 are extrapolated to 6.2 Mbps and 7.6 Mbps, respectively. Meanwhile, the data rate of D-UE 2 is extrapolated to 4.5 Mbps.

Referring to Figure 4(b), in the downlink, the BS sends the data to the two C-UEs; at the same time, D-UE 2 sends data to D-UE 1. Figure 8 presents the constellation of the demodulated signals at the two C-UEs and D-UE 1, as well as their EVMs. Based on the measured EVM, the downlink data rates of C-UE 1 and C-UE 2 are extrapolated to 5.3 Mbps and

TABLE III: EVM specification in IEEE 802.11ac [39].

EVM (dB)	(inf,-5)	[-5,-10)	[-10,-13)	[-13,-16)	[-16,-19)	[-19,-22)	[-22,-25)	[-25,-27)	[-27,-30)	[-30,-32)	[-32,-inf)
Modulation	N/A	BPSK	QPSK	QPSK	16QAM	16QAM	64QAM	64QAM	64QAM	256QAM	256QAM
Coding rate	N/A	1/2	1/2	3/4	1/2	3/4	2/3	3/4	5/6	3/4	5/6
γ(EVM)	0	0.5	1	1.5	2	3	4	4.5	5	6	20/3

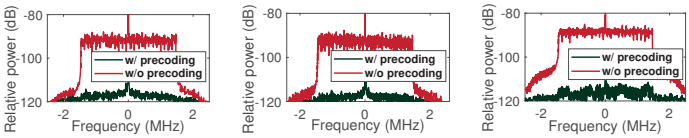

(a) Received interference at C-UE 1. (b) Received interference at C-UE 2. (c) Received interference at D-UE 1.

Fig. 9: Received interference at the receiving nodes in the downlink with and without beamforming at the transmitters.

6.2 Mbps, respectively. Meanwhile, the data rate of D-UE 1 is extrapolated to 4.6 Mbps.

Beamforming Capability: Referring to Figure 4(b), in the downlink, we examine the effectiveness of beamforming at the two transmitters (BS and D-UE 2) . To do so, we measure interference at the receiving nodes (C-UE 1, C-UE 2, and D-UE 1) in two cases: with and without beamforming. For the case without beamforming, we use precoder $[1/2,\ 1/2,\ 1/2,\ 1/2]$ at the BS and $[1/\sqrt{3},\ 1/\sqrt{3},\ 1/\sqrt{3}]$ at D-UE 2. Figure 9 presents the measured interference at the receiving nodes. It is evident that the proposed beamforming methods can very effectively pre-cancel interference. Specifically, both beamforming methods achieve at least 28.5 dB interference cancellation capability. Thanks to the effective beamforming methods, both MU-MIMO and D2D subsystems can achieve superior performance in the downlink, as shown in Figure 8.

D. DM-COM vs. Cellular-MU-MIMO and Full-MU-MIMO

By the same token in the case study, we now study the performance of DM-COM by placing the two D-UEs at 50 different locations as shown in Figure 6. In this study, we use Cellular-MU-MIMO and Full-MU-MIMO as the comparison baselines (see Figure 5).

EVM Distribution: Figure 10 presents the distribution of measured EVM when the three schemes are used. Specifically, Figure 10(a) presents the measured EVM of demodulated signals at the BS in the uplink MU-MIMO when DM-COM, Cellular-MU-MIMO, and Full-MU-MIMO are respectively used. Particularly, we considered two cases for DM-COM: (i) D2D subsystem uses NR-like PHY and (ii) D2D subsystem uses WiFi-like PHY. From the figure, we can see that DM-COM achieves -26.1 dB EVM on average, no matter which PHY (5G NR or WiFi) is used for D2D communications. In contrast, Cellular-MU-MIMO achieves about -27.6 dB EVM on average, and Full-MU-MIMO achieves -20.1 dB EVM on average. The EVM gap between DM-COM and Cellular-MU-MIMO is only 1.5 dB. This means that, in DM-COM, the EVM degradation at the BS caused by interference from D2D subsystem is only 1.5 dB.

Figure 10(b) presents the measured EVM of the demodulated signals at the two C-UEs in the downlink MU-MIMO.

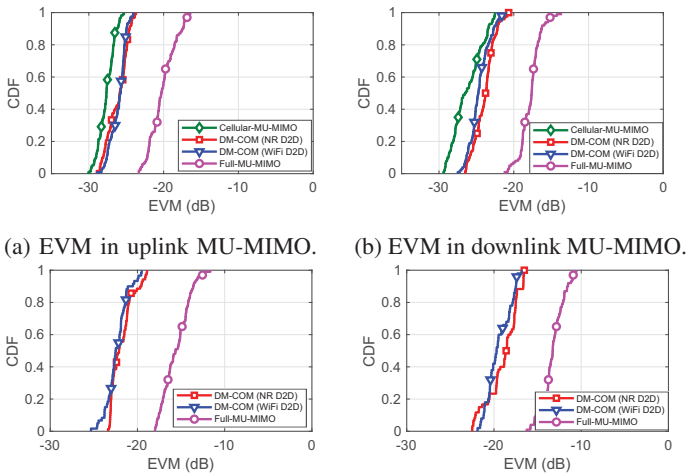

(a) EVM in uplink MU-MIMO. (b) EVM in downlink MU-MIMO.

(c) EVM in forward D2D. (d) EVM in backward D2D.

Fig. 10: EVM distribution of demodulated signals when DM-COM, Cellular-MU-MIMO, and Full-MU-MIMO are used.

It shows that DM-COM achieves an average of -24.3 dB EVM in the downlink MU-MIMO. The EVM gap between DM-COM and Cellular-MU-MIMO is about 1.9 dB. This means that, in DM-COM, the EVM degradation at C-UEs caused by interference from D2D subsystem is only 1.9 dB.

Figure 10(c) and (d) present the measured EVM in forward and backward D2D transmissions when DM-COM and Full-MU-MIMO are used. Note that Cellular-MU-MIMO does not support D2D communication, and thus these two figures do not include the results from Cellular-MU-MIMO. On average, DM-COM achieves -22.1 dB EVM for forward D2D transmission and -19.2 dB EVM for backward D2D transmission, no matter which PHY (NR or WiFi) is used for D2D subsystem. In contrast, Full-MU-MIMO achieves -15.6 dB EVM for forward D2D transmission and -13.2 dB EVM for backward D2D transmission. This means that DM-COM outperforms Full-MU-MIMO by 6.5 dB in forward D2D communication and 6.0 dB in backward D2D communication.

Per-UE Throughput Distribution: We extrapolate per-UE throughput (data rate) based on the measured EVM. Figure 11 presents the results. The staircase shape of the curves stems from the MCS selection, which yields discrete data rate region in nature. On average, DM-COM achieves 6.7 Mbps per-UE throughput in uplink MU-MIMO and 6.1 Mbps per-UE throughput in downlink MU-MIMO. At the same time, it achieves 5.4 Mbps for forward D2D transmission and 4.2 Mbps for backward D2D transmission.

E. Summary of Observations

Figure 12 presents the total throughput of MU-MIMO and D2D subsystems when DM-COM, Cellular-MU-MIMO, and Full-MU-MIMO are used. The total throughput of MU-MIMO is the summation of its uplink and downlink data rates. The total throughput of D2D is the summation of its backward and forward data rates. The total throughput are averaged over the 50 different locations in Figure 6.

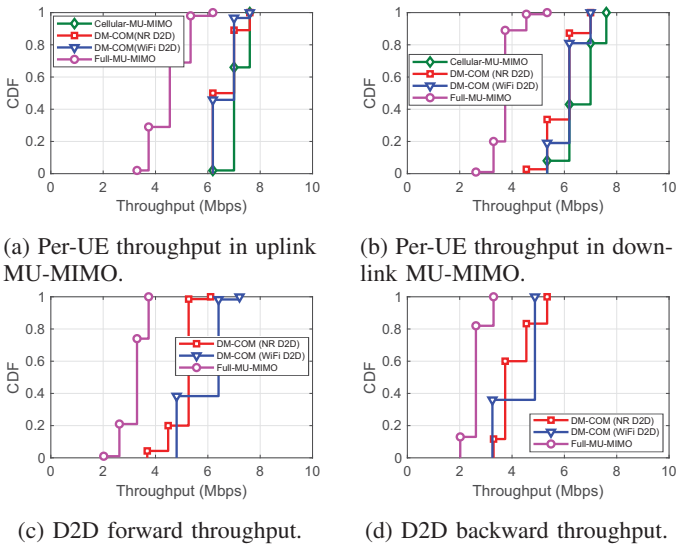

(a) Per-UE throughput in uplink MU-MIMO.

(b) Per-UE throughput in downlink MU-MIMO.

(c) D2D forward throughput.

(d) D2D backward throughput.

Fig. 11: Distribution of extrapolated throughput when DM-COM, Cellular-MU-MIMO, and Full-MU-MIMO are used.

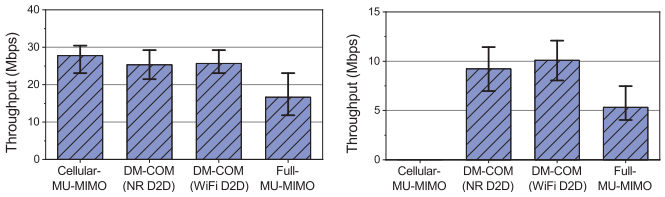

(a) Total throughput of MU-MIMO. (b) Total throughput of D2D.

Fig. 12: Total throughput of the MU-MIMO and D2D subsystems when DM-COM, Cellular-MU-MIMO and Full-MU-MIMO are respectively used.

MU-MIMO subsystem: Figure 12(a) shows that DM-COM achieves 25.3 Mbps throughput for MU-MIMO subsystem when using 5G NR PHY for D2D and 25.7 Mbps throughput when using WiFi PHY for D2D. In contrast, Cellular-MU-MIMO achieves 27.8 Mbps throughput for MU-MIMO. This means that, in DM-COM, the throughput degradation of C-UEs caused by interference from D-UEs is only 8%. Full-MU-MIMO achieves 16.6 Mbps, which is much less than DM-COM.

D2D subsystem: Figure 12(b) shows that DM-COM achieves 9.2 Mbps throughput for D2D subsystem when using 5G NR PHY and 10.1 Mbps throughput when using WiFi PHY. Recall that the system bandwidth is 5 MHz. This means that DM-COM achieves more than 1.9 bit/s/Hz spectral efficiency for D2D communication. In contrast, Full-MU-MIMO achieves 5.3 Mbps throughput for D2D. This means that DM-COM outperforms Full-MU-MIMO by 82%. This can be partially attributed to the two-hop D2D communication in Full-MU-MIMO.

VIII. Conclusion

In this paper, we presented DM-COM, a practical scheme that combines D2D and MU-MIMO technologies to advance cellular networks. The main challenge in DM-COM is managing interference between D2D and MU-MIMO subsystems. DM-COM takes the advantage of multiple antennas on the network devices to cancel interference and recover the desired signals, without requiring channel state information and fine-grained network-wide synchronization. This was achieved through the design of practical, yet effective, multi-user detection and beamforming methods. We have built a prototype of DM-COM on a custom-built wireless testbed and compared its performance with two existing schemes. Our experimental results show that DM-COM achieves 1.9 bit/s/Hz spectral efficiency for D2D users. Moreover, the throughput degradation of MU-MIMO users due to the spectrum utilization of D2D users is less than 8%.

Appendix A
Proof of Lemma 1

We denote $\mathbf{H}(k)$ as the compound channel between the BS and all the transmitting UEs over subcarrier k, i.e., $\mathbf{H}(k) = \begin{bmatrix}\mathbf{H}_{\rm c}(k) & \mathbf{H}_{\rm d_1}(k)\end{bmatrix}$; we also denote $\mathbf{S}(l,k)$ as the compound transmit signals at all C-UEs and D-UE 1, i.e., $\mathbf{S}(l,k) = \begin{bmatrix}\mathbf{s}_{\rm c}(l,k) & \mathbf{s}_{\rm d_1}(l,k)\end{bmatrix}^T$. Then, we can re-write (2) over subcarrier k and OFDM symbol l as:

$$\mathbf{Y}(l,k) = \mathbf{H}(k)\mathbf{S}(l,k). \tag{7}$$

As the auto-correlation matrix of the compound transmit signals, we have

$$\mathbf{R}_{\rm S} = \mathbb{E}(\mathbf{S}\mathbf{S}^H) \overset{(a)}{=} \begin{bmatrix}\mathbf{R}_{\rm c} & \mathbf{0}\\ \mathbf{0} & \mathbf{R}_{\rm d}\end{bmatrix} \overset{(b)}{=} \begin{bmatrix}\mathbf{I} & \mathbf{0}\\ \mathbf{0} & \mathbf{R}_{\rm d}\end{bmatrix} \tag{8}$$

where $\mathbf{R}_{\rm S}$, $\mathbf{R}_{\rm c}$, and $\mathbf{R}_{\rm d}$ are the auto-correlation matrix of the compound transmit signals, auto-correlation matrix of C-UEs' transmit signals, and auto-correlation matrix of D-UE 1 transmit signals, respectively. Equality (a) follows from the fact that the transmit signal from C-UEs are independent of the transmit signals from D-UE 1. Also, (b) follows from the fact that transmit signals from C-UEs are independent too.

Based on (3), (7), and (8), we obtain the approximate-MMSE MIMO detector $\mathbf{G}(k)$ over subcarrier k as follows:

$$\begin{aligned}\mathbf{G}(k) &= \Big[\sum_{(l,k')\in\mathcal{R}} \mathbf{Y}(l,k')\mathbf{Y}(l,k')^{\mathsf{H}}\Big]^{+}\Big[\sum_{(l,k')\in\mathcal{R}} \mathbf{Y}(l,k')\mathbf{s}_{\rm c}(l,k')^{\mathsf{H}}\Big]\\ &= \mathbb{E}\big[\mathbf{Y}(l,k)\mathbf{Y}(l,k)^{\mathsf{H}}\big]^{+}\mathbb{E}\big[\mathbf{Y}(l,k)\mathbf{s}_{\rm c}(l,k)^{\mathsf{H}}\big]\\ &= \big[\mathbf{H}(k)\mathbf{R}_{\rm S}\mathbf{H}(k)^{\mathsf{H}}\big]^{+}\big[\mathbf{H}(k)\mathbf{I}'\big],\end{aligned} \tag{9}$$

where $\mathbf{I}'$ is a matrix which its entries on the diameter are one and other entries are zero. Then, we have

$$\begin{aligned}\hat{\mathbf{s}}_{\rm c}(l,k) &= \mathbf{G}(k)^{*}\mathbf{Y}(l,k)\\ &= \Big\{\big[\mathbf{H}(k)\mathbf{R}_{\rm S}\mathbf{H}(k)^{\mathsf{H}}\big]^{+}\big[\mathbf{H}(k)\mathbf{I}'\big]\Big\}^{\mathsf{H}}\mathbf{H}(k)\mathbf{S}(l,k)\\ &= \mathbf{s}_{\rm c}(l,k), \quad \forall l,k.\end{aligned} \tag{10}$$

This means that the approximate-MMSE MIMO detector $\mathbf{G}(k)$ is capable of perfectly recovering the original signal over subcarrier k and OFDM symbol l in a noise-free environment.

APPENDIX B
PROOF OF LEMMA 2

Referring to Fig. 2, D-UE 1 first remains silent for a while, and D-UE 2 merely receives interfering signals from N C-UEs. Then, D-UE 2 uses the overheard interference to design precoding filter for pre-canceling its generated interference at C-UEs in backward transmission. The received interference can be written as:

$$\mathbf{y}_{\mathrm{d}}(k) = \mathbf{H}_{\mathrm{dc}}(k)\mathbf{s}_{\mathrm{c}}(k), \tag{11}$$

where $\mathbf{H}_{\mathrm{dc}}(k)$ denotes the compound channel between D-UE 2 and all the C-UEs over subcarrier k. Then, we have

$$\mathbb{E}[\mathbf{y}_{\mathrm{d}}(k)\mathbf{y}_{\mathrm{d}}(k)^{\mathsf{H}}] \overset{(a)}{=} \mathbf{H}_{\mathrm{dc}}^{[1]}(k)\mathbf{H}_{\mathrm{dc}}^{[1]}(k)^{\mathsf{H}}, \tag{12}$$

where (a) follows from the fact that $\mathbb{E}[\mathbf{s}_{\mathrm{c}}(k)\mathbf{s}_{\mathrm{c}}(k)^{\mathsf{H}}] = \mathbf{I}$ as the N C-UEs send N independent data streams. Recall that $N + d \leq M_{\mathrm{d2}}$ and consequently $d \leq M_{\mathrm{d2}} - N$. Based on the right hand side of (12), rank of $\mathbb{E}[\mathbf{y}_{\mathrm{d}}(l,k)\mathbf{y}_{\mathrm{d}}(l,k)^{\mathsf{H}}]$ is at most N. The rank reduces when channel is correlated and rank deficient. Therefore, $\mathrm{svd}(\mathbf{y}_{\mathrm{d}}(k)\mathbf{y}_{\mathrm{d}}(k)^{\mathsf{H}})$ has at least d zero singular vectors. If $\mathbf{u}_i$ denotes the ith left singular vector, based on (12), we have

$$\Big(\mathbf{H}_{\mathrm{dc}}(k)\mathbf{H}_{\mathrm{dc}}(k)^{\mathsf{H}}\Big)\mathbf{u}_i = \mathbf{0}, \quad M_{\mathrm{d2}} - d + 1 \leq i \leq M_{\mathrm{d2}}. \tag{13}$$

If channel reciprocity is maintained with the aid of a channel calibration method, $\mathbf{H}_{\mathrm{cd}}(k) = \big(\mathbf{H}_{\mathrm{dc}}(k)\big)^T$. Then, it is easy to show that $\mathbf{H}_{\mathrm{cd}}(k)\mathbf{P} = \mathbf{0}$. This completes the proof.

REFERENCES

[1] C. Lim, T. Yoo, B. Clerckx, B. Lee, and B. Shim, "Recent trend of multiuser MIMO in LTE-advanced," *IEEE Commun. Mag.*, vol. 51, no. 3, pp. 127–135, 2013.

[2] S. Zhang, J. Liu, H. Guo, M. Qi, and N. Kato, "Envisioning device-to-device communications in 6G," *IEEE Network*, vol. 34, no. 3, pp. 86–91, 2020.

[3] M. Waqas, Y. Niu, Y. Li, M. Ahmed, D. Jin, S. Chen, and Z. Han, "A comprehensive survey on mobility-aware D2D communications: Principles, practice and challenges," *IEEE Commun. Surveys Tuts.*, vol. 22, no. 3, pp. 1863–1886, 2019.

[4] U. Uyoata, J. Mwangama, and M. Dlodlo, "Robust beamforming for D2D multicast communication," *Physical Communication*, vol. 43, p. 101217, 2020.

[5] Y.-S. Wang, Y.-W. P. Hong, and W.-T. Chen, "Dynamic transmission policy for multi-pair cooperative device-to-device communication with block-diagonalization precoding," *IEEE Trans. Wireless Commun.*, 2019.

[6] J. Mirza, G. Zheng, K.-K. Wong, and S. Saleem, "Joint beamforming and power optimization for D2D underlaying cellular networks," *IEEE Trans. Veh. Technol.*, vol. 67, no. 9, pp. 8324–8335, 2018.

[7] J. Tan, Y.-C. Liang, L. Zhang, and G. Feng, "Deep reinforcement learning for joint channel selection and power control in D2D networks," *IEEE Trans. Wireless Commun.*, 2020.

[8] Y. Chen, B. Ai, Y. Niu, K. Guan, and Z. Han, "Resource allocation for device-to-device communications underlaying heterogeneous cellular networks using coalitional games," *IEEE Trans. Wireless Commun.*, vol. 17, no. 6, pp. 4163–4176, 2018.

[9] J. Kim, T. Kim, M. Hashemi, C. G. Brinton, and D. J. Love, "Joint optimization of signal design and resource allocation in wireless D2D edge computing," in *Proc. IEEE INFOCOM*, pp. 2086–2095, 2020.

[10] B. Özbek, M. Pischella, and D. Le Ruyet, "Energy efficient resource allocation for underlaying multi-D2D enabled multiple-antennas communications," *IEEE Trans. Veh. Technol.*, 2020.

[11] X. Wang, T. Jin, L. Hu, and Z. Qian, "Energy-efficient power allocation and Q-learning-based relay selection for relay-aided D2D communication," *IEEE Trans. on Veh. Technol.*, vol. 69, no. 6, pp. 6452–6462, 2020.

[12] J. Huang, C.-c. Xing, and M. Guizani, "Power allocation for D2D communications with SWIPT," *IEEE Trans. Wireless Commun.*, 2020.

[13] X. Li, R. Shankaran, M. A. Orgun, G. Fang, and Y. Xu, "Resource allocation for underlay D2D communication with proportional fairness," *IEEE Trans. Veh. Technol.*, vol. 67, no. 7, pp. 6244–6258, 2018.

[14] J. Huang, S. Huang, C.-C. Xing, and Y. Qian, "Game-theoretic power control mechanisms for device-to-device communications underlaying cellular system," *IEEE Trans. Veh. Technol.*, vol. 67, no. 6, pp. 4890–4900, 2018.

[15] R. AliHemmati, B. Liang, M. Dong, G. Boudreau, and S. H. Seyedmehdi, "Power allocation for underlay device-to-device communication over multiple channels," *IEEE Trans. Signal Inf. Process. Netw.*, vol. 4, no. 3, pp. 467–480, 2018.

[16] R. AliHemmati, M. Dong, B. Liang, G. Boudreau, and S. H. Seyedmehdi, "Multi-channel resource allocation toward ergodic rate maximization for underlay device-to-device communications," *IEEE Trans. Wireless Commun.*, vol. 17, no. 2, pp. 1011–1025, 2018.

[17] C.-Y. Chen, C.-A. Sung, and H.-H. Chen, "Capacity maximization based on optimal mode selection in multi-mode and multi-pair D2D communications," *IEEE Trans. Veh. Technol.*, vol. 68, no. 7, pp. 6524–6534, 2019.

[18] S. Badri and M. Rasti, "Interference management and duplex mode selection in in-band full duplex D2D communications: A stochastic geometry approach," *IEEE Trans. Mobile Comput.*, 2020.

[19] J. Huang, J. Cui, C.-C. Xing, and H. Gharavi, "Energy-efficient SWIPT-empowered D2D mode selection," *IEEE Trans. Veh. Technol.*, 2020.

[20] J. Lyu, H.-M. Wang, and K.-W. Huang, "Physical layer security in D2D underlay cellular networks with poisson cluster process," *IEEE Trans. Commun.*, vol. 68, no. 11, pp. 7123–7139, 2020.

[21] B. Seok, J. C. S. Sicato, T. Erzhena, C. Xuan, Y. Pan, and J. H. Park, "Secure D2D communication for 5G IoT network based on lightweight cryptography," *Applied Sciences*, vol. 10, no. 1, p. 217, 2020.

[22] C. Suraci, S. Pizzi, D. Garompolo, G. Araniti, A. Molinaro, and A. Iera, "Trusted and secured D2D-aided communications in 5G networks," *Ad Hoc Networks*, p. 102403, 2021.

[23] L.-N. Tran, M. Bengtsson, and B. Ottersten, "Iterative precoder design and user scheduling for block-diagonalized systems," *IEEE Trans. signal process.*, vol. 60, no. 7, pp. 3726–3739, 2012.

[24] V.-D. Nguyen, L.-N. Tran, T. Q. Duong, O.-S. Shin, and R. Farrell, "An efficient precoder design for multiuser MIMO cognitive radio networks with interference constraints," *IEEE Trans. Veh. Technol.*, vol. 66, no. 5, pp. 3991–4004, 2017.

[25] S. Dadallage, C. Yi, and J. Cai, "Joint beamforming, power, and channel allocation in multiuser and multichannel underlay MISO cognitive radio networks," *IEEE Trans. Veh. Technol.*, vol. 65, no. 5, pp. 3349–3359, 2016.

[26] W. Wang, R. Wu, and J. Liang, "ADS-B signal separation based on blind adaptive beamforming," *IEEE Trans. Veh. Technol.*, vol. 68, pp. 6547–6556, July 2019.

[27] M. H. Al-Ali and K. Ho, "Transmit precoding in underlay MIMO cognitive radio with unavailable or imperfect knowledge of primary interference channel," *IEEE Trans. Wireless Commun.*, vol. 15, no. 8, pp. 5143–5155, 2016.

[28] S.-M. Cai and Y. Gong, "Cognitive beamforming for throughput maximization with statistical cross channel state information," *IEEE Commun. Lett.*, vol. 18, no. 11, pp. 2031–2034, 2014.

[29] Y. Noam and A. J. Goldsmith, "Blind null-space learning for MIMO underlay cognitive radio with primary user interference adaptation," *IEEE Trans. Wireless Commun.*, vol. 12, no. 4, pp. 1722–1734, 2013.

[30] S. Amuru, "Beam learning–using machine learning for finding beam directions," *arXiv preprint arXiv:1906.04368*, 2019.

[31] Y. Noam and A. J. Goldsmith, "The one-bit null space learning algorithm and its convergence," *IEEE Trans. Signal Process.*, vol. 61, no. 24, pp. 6135–6149, 2013.

[32] P. Botsinis, D. Alanis, Z. Babar, S. X. Ng, and L. Hanzo, "Iterative quantum-assisted multi-user detection for multi-carrier interleave division multiple access systems," *IEEE Trans. Commun.*, vol. 63, no. 10, pp. 3713–3727, 2015.

[33] Y. Du, B. Dong, Z. Chen, X. Wang, Z. Liu, P. Gao, and S. Li, "Efficient multi-user detection for uplink grant-free NOMA: Prior-information aided adaptive compressive sensing perspective," *IEEE J. Sel. Areas Commun.*, vol. 35, no. 12, pp. 2812–2828, 2017.

[34] J. Zhang, S. Chen, X. Mu, and L. Hanzo, "Turbo multi-user detection for OFDM/SDMA systems relying on differential evolution aided iterative channel estimation," *IEEE Trans. Commun.*, vol. 60, no. 6, pp. 1621–1633, 2012.

[35] M. Wu, B. Yin, G. Wang, C. Dick, J. R. Cavallaro, and C. Studer, "Large-scale MIMO detection for 3GPP LTE: Algorithms and FPGA implementations," *IEEE J. Sel. Topics Signal Process.*, vol. 8, no. 5, pp. 916–929, 2014.
[36] G. T. 38.211, "Nr; physical channels and modulation," *3rd Generation Partnership Project; Technical Specification Group Radio Access*, 2017.
[37] Y. Shi, J. Liu, C. Jiang, C. Gao, and Y. T. Hou, "A DoF-based link layer model for multi-hop MIMO networks," *IEEE Trans. Mobile Comput.*, vol. 13, no. 7, pp. 1395–1408, 2014.
[38] C. Shepard, H. Yu, N. Anand, E. Li, T. Marzetta, R. Yang, and L. Zhong, "Argos: Practical many-antenna base stations," in *Proc. ACM Int. Conf. Mobile Comput. Netw. (MobiCom)*, pp. 53–64, 2012.
[39] IEEE 802.11ac, "IEEE standard for information technology local and metropolitan area networks part 11: Wireless LAN medium access control (MAC) and physical layer (PHY) specifications amendment 5: Enhancements for higher throughput," *IEEE Standards 802.11ac*, 2014.
[40] M. T. Kawser, N. I. B. Hamid, M. N. Hasan, M. S. Alam, and M. M. Rahman, "Downlink SNR to CQI mapping for different multiple-antenna techniques in LTE," *Int. J. Inf. Electron. Eng.*, vol. 2, no. 5, p. 757, 2012.
[41] T. ETSI, "136 213 v12. 3.0 technical specification LTE," *Evolved Universal Terrestrial Radio Access (E-UTRA)*.